Enhancement of photocatalytic properties of nanosized La2Ti2O7 synthesized by glycine-assisted sol-gel route

Sébastien Leroy, Jean-François Blach, Agnieszka Kopia, Sebastian Lech, Łukasz Cieniek, Nicolas Kania, S. Saitzek

Enhancement of the photocatalytic properties of nanosized $La_2Ti_2O_7$ synthesized by Glycine-assisted sol-gel route

Sébastien Leroy[1], Jean-François Blach[1], Agnieszka Kopia[2], Sebastian Lech[2], Łukasz Cieniek[2], Nicolas Kania[1], Sébastien Saitzek[1].

[1] Univ. Artois, CNRS, Centrale Lille, ENSCL, Univ. Lille, UMR 8181, Unité de Catalyse et Chimie du Solide (UCCS), F-62300 Lens, France

[2] AGH-University of Science and Technology, al. A. Mickiewicza 30, 30-059 Krakow, Poland

Abstract

Nanosized lanthanum titanate ($La_2Ti_2O_7$) have been synthetized by a new glycine-assisted sol gel route in order to improve the photocatalytic properties. The effect of calcination temperature on crystallites size and their photocatalytic efficiency has been investigated, showing a best efficiency for a calcination temperature of 1000°C. Thus, the apparent rate constant of degradation of rhodamine B is greatly improved by a factor of 1.86 compared to commercial P25 TiO_2 Degussa® and by a factor of 6.42 compared to a sol-gel synthesis without glycine.

In order to study the efficiency of the photocatalyst on industrial water discharges, the photodegradation of phenol has also been investigated, showing the effectiveness of the photocatalyst with an apparent rate constant of 5.49×10^{-3} min^{-1}. The photocatalyst mass loading, the luminous flux received and the pH have been also investigated. The effect of different type of scavengers shows the importance of superoxide and hole in the photodegradation mechanisms. Finally, the coupling of ultrasound and light excitation was carried out in order to achieve a sonophotocatalysis effect. The apparent rate constant corresponding to the photodegradation of phenol increases slightly. Nevertheless, we have been able to observe that this is more important as the volume of the photoreactor is low.

Corresponding author:
Pr. Sébastien SAITZEK,
[1]Université d'Artois, Unité de Catalyse et de Chimie du Solide, UCCS,
Équipe Chimie du Solide, CNRS-UMR 8181, Faculté des Sciences Jean Perrin,
F-62300 LENS, France
Phone: +33 / 321791732, Fax: +33 / 321177955, E-mail: sebastien.saitzek@univ-artois.fr

1. Introduction

For a few decades, the development of new photocatalysts has been significant interest in the scientific community for their many potential applications, including: i) the photodegradation of organic pollutants such as dyes[1–4], pharmaceutical wastes[5,6], industrial wastewater treatment[7], mineralization of hazardous organic product[8], agricultural wastewater treatment (pesticides) [9,10], polymer fibers degradation[11], ii) the hydrogen production by water-splitting[12,13], iii) the photocatalytic redox reactions, for example the reduction of Cr(VI) to Cr(III)[14] or for the direct formation of metallic nanoparticles by photoreduction[15] and iv) the development of anti-bacterial coating based on the production of Reactive Oxygen Species (ROS) at the photocatalyst surface[16]. Among the photocatalyst oxides, TiO_2 is widely used and studied [17–19] due to its good chemical stability, nontoxicity, abundance of raw materials and strong oxidizing ability[20]. However, the growing interest has led researchers to explore new photocatalytic materials such as semiconductors ZnO[2], SnO_2[21], WO_3[22], ZnS[23], $BiVO_4$[24], $BiPO_4$[25], and $La_2Ti_2O_7$[26,27] (LTO) in order to probe their effectiveness under UV light. Currently, these studies are being continued to allow use under visible irradiation, for example by i) band gap engineering via crystallites shape control[28], stress/strain effect[29] or even by the development of a compound with a mixed anion such as oxynitrides[30], oxyfluorides[31], oxyhydride,… ; ii) the effect of Localized Surface Plasmon Resonance (LSPR) via metallic nanoparticles as Au or Ag[32]; iii) The combination of light-absorbing materials such as $CdS/La_2Ti_2O_7$ nanocomposites[33] or g-$C_3N_4/La_2Ti_2O_7$[34] and iv) the creation of all oxide n/p heterojunction such as $BiOI/La_2Ti_2O_7$[35] or $SnS_2/La_2Ti_2O_7$[36]. The ability of $La_2Ti_2O_7$ to act as a photocatalyst has been highlighted since the early 2000s but this oxide has been known since the 1970s for these piezo-electric properties[37]. Lanthanum dititanate oxide belongs to the layered perovskite structure with a general formula $A_nB_nO_{3n+2}$ with (A=La et B=Ti). The $La_2Ti_2O_7$, so-called LTO

is characterised by a stack of 4 layers of [TiO_6] octahedron along the c axis and infinite layers of octahedra belong a and b axis. In 1975, Gasperin *et al.*[38] resolve the structure of $La_2Ti_2O_7$, highlighting a monoclinic structure with a $P2_1$ space group whose lattice parameters are: a= 7.800(3) Å ; b= 5.546(2) Å ; c= 13.011(4) Å et β= 98.60(2)°. At 780°C, this monoclinic phase evolves to an orthorhombic structure ($CmC2_1$ space group with following lattice parameters : a = 3.954(2) Å ; b = 5.607(2) Å et c = 25.952(8) Å[39]) while retaining ferroelectric properties. These are then lost when the temperature becomes higher than T_c = 1482°C[40] and the structure evolves again towards an orthorhombic structure with *Cmcm* space group (paraelectric phase). LTO is a ferro-/piezo-electric material with a high Curie temperature[41], allowing use in extreme environments as piezoelectric actuators for aeronautic or spatial applications[42]. Beyond their electronic applications, LTO can also be used as a host matrix for the development of luminescent materials. Indeed, a substitution of the site La, by another element whose near ionic radius is possible without structure modification. So, LTO acts as an excellent host matrix, especially for the substitution of lanthanides ions such as Pr^{3+} [43,44], Eu^{3+} [45,46], Sm^{3+} [47,48],… . In addition, a substitution of $La_2Ti_2O_7$ with Er^{3+} has made it possible to obtain an up conversion luminescence properties which may be of interest for improving the efficiency of solar cells[49,50] for phototherapy applications[51]. More recently, co-substitution also makes it possible to couple the two properties of classical luminescence and up-conversion to produce sensors sensitive to a double excitation[52].

In addition, $La_2Ti_2O_7$ oxide has been studied for its activity in water-splitting either alone [53] or co-catalyzed with metals [54], [55], for photocatalytic degradation of organic pollutants CH_3Cl [56], CH_3OH [57] and dyestuff [27], [58], [59], [60], for photodegradation of antibiotics molecules such as ofloxacin [61] and the oxidation of isopropanol [62].

In a previous work[27], we used $La_2Ti_2O_7$ synthesized by Sol-Gel method and investigated its photocatalytic properties on the Rhodamine B photodegradation followed by the study of the influence the influence of various parameters such as temperature, catalyst loading, pH. We have demonstrated an efficient use of this oxide for photocatalysis processes under UV irradiation.

However, the photocatalytic efficiency is strongly affected by the degree of crystallinity and the exchange surface of the material. In recent years, the optimization of synthetic parameters in order to control the size of crystallites and their crystallinity have been the subject of much researches by the scientific community, in particular via: i) the nature of precursors employed [63], ii) the use of polymer precursors for porosity control[61] ; ii) the diversification of synthesis processes such as the hydrothermal route [64], the polymeric sol-gel route [65],[66], microwave assisted synthesis[67], Molten Salt Synthesis (MSS)[68], spray pyrolysis and others ; iii) the use of template[69] or iv) the design of microreactors at the nanometric scale[70].

In this present work, we have sought to improve the photocatalytic activity by developing a new synthetic route limiting the coalescence of grains in the calcination step. For that, $La_2Ti_2O_7$ were synthesized by a new route named Sol-Gel method assisted by glycine combustion. Firstly, we will demonstrate the improvement of the photocatalytic properties with respect to the sol-gel synthesis already described. Secondly, for further understanding of photodegradation mechanism performed on Rhodamine B and phenol pollutants, we used scavenger species and studied photodegradation kinetics by total organic carbon measurements. The photocatalytic properties were studied as a function of catalyst loading, pH and luminous flux. Finally, a study in sonophotocatalysis was made by highlighting the influence of volume and the increase of catalytic efficiency.

2. Experimental section

Nanosized $La_2Ti_2O_7$ oxide was synthesized by Sol-Gel method assisted by glycine combustion. Lanthanum (II) nitrate hexahydrate (Strem Chemicals, 99,99%), glycine (Acros Organics 99%) and Titanium (IV) n-butoxide (Alfa Aesar 98 + %) were used as starting precursors. First, a solution (A) was prepared according to the following protocol: 0.15 mol of lanthanum nitrate initially ground manually in an agate mortar is introduced into a mixture containing 10 mL of water and 10 mL of acetic acid. After 15 min of stirring, 0.30 mol of glycine is introduced into the reaction vessel of A solution and then homogenized for 15 min by stirring. At the same time, a second solution (B) was prepared by dissolving 0.15 mol of titanium precursor in 10 mL of absolute ethanol. The whole is homogenized by stirring for 15 min. Finally, A and B solutions were mixed and stirred for 30 min until a translucent gel was obtained. The solution was then placed in oven at 80°C until a viscous white gel was formed. This gel is then calcined in air at different temperatures for 10h to obtain $La_2Ti_2O_7$ nanopowders.

X-ray diffraction (XRD) patterns were collected using a Rigaku ULTIMA IV diffractometer equipped with Cu anticathode, Soller slits to limit the divergence of X-ray beam and a nickel foil filter attenuates the Cu K_β line. The registered angular range is 20°-80° (scanning rate of 0.1°. min^{-1}) using the Bragg-Brentano configuration. In order to estimate the average crystallite size, we used Scherrer's relation[71,72]:

$$D = \frac{K\lambda}{FWHM_s \cos\theta} \qquad (1)$$

Where λ is the X-ray wavelength ($\lambda\overline{K}_\alpha$(Cu) = 1.5418 Å), $FWHM_s$ corresponds to the broadening only induced by the size effect, which is deconvolved from the instrumental part, K is a dimensionless shape factor (with a typical value of 0.89) and θ is Bragg's angle corresponding to (*hkl*) reflection.

Transmission electron microscopy (TEM) examinations were performed using Tecnai G2-20 TWIN FEI microscope, equipped with a LaB_6 cathode and operating at the accelerating voltage of 200 kV.

The surface morphology and the chemical composition of the powder was analysed using Scanning Electron Microscope (FEI Nova NanoSEM 450) equipped with Energy Dispersive Spectroscopy detector Octane Elect Plus (EDAX) working with GENESIS software. Optical band gaps were calculated from the absorbance spectra recorded on UV-2600 spectrophotometer with integrating sphere (Shimadzu). For that, the Tauc plot based on following equation has been used[73,74]:

$$\alpha h\nu = A\,(h\nu - Eg)^{n} \qquad (2)$$

Where α is the absorption coefficient, hν corresponds to photon energy, A is a proportionality constant, E_g is the optical band gap, and the exponent n is a factor linked to the nature of the transition (n = ½ for direct transition).

Porosity measurements were determined by nitrogen adsorption at -196 °C on a Tristar II apparatus from Micromeritics, after having degassed the sample under vacuum at 120°C. The specific surface areas (S_{BET}) were calculated from the Brunauer–Emmett–Teller (BET) equation using P/P_0 values in the 1.0×10^{-2} and 2.5×10^{-1} range and the pore size distributions were obtained from the desorption branch using the Barrett–Joyner–Halenda (BJH) method. Each specific surface area measurement was performed on three consecutive batches of the same sample. The S_{BET} values uncertainty is estimated to be less than 5%. Total Organic Carbon (TOC) analyses were carried out on a TOC-L total organic carbon analyzer (Shimadzu). The values presented are the averages obtained on 3 consecutive measurements.

The photocatalytic activity was determined by monitoring the degradation of Rhodamine B and phenol on UV-visible spectra using a usual Beer-Lambert law. The used photo-reactor consist of a 200 mL flask irradiated from above by a 40 W UV lamp (254 nm)

and an aluminium foil covers the system to prevent UV radiations. Before any measurements, the solution was stirred for 30 min in the dark in presence of catalyst to ensure an appropriate adsorption/desorption equilibrium. To describe the photocatalytic kinetic at solid-liquid interface the Langmuir-Hinshelwood (LH) model was used [27],[75]. In such model, it is commonly admitted that the reaction products and intermediates are negligible and that the rate of reaction depends directly to the coverage surface of the catalytic site (θ). This model also allows to consider the relative adsorption on the surface oxide and the photodegradation rate v can be expressed as follow:

$$v = k_{ph}\theta \; with \; \theta = \frac{K_{LH}C}{1+K_{LH}C} \qquad (3)$$

Where k_{ph} is the kinetic constant of photodegradation, K_{LH} the adsorption constant which depends on the affinity between dye and catalyst and C the initial concentration of dye. For low adsorption and/or low concentration (i.e. $K_{LH}C<<1$) the photodegradation rate become directly proportional to the dye concentration and can be expressed as follow:

$$v = k_{ph}K_{LH}C = k_{app}C \qquad (4)$$

Where k_{app} is the apparent rate constant of the first order reaction and can be determine by the slope of the straight line when plotting $Ln(C_0/C)$ *vs* t.

3. Results and discussions

3.1. Structural characterizations

XRD patterns of obtained $La_2Ti_2O_7$ are shown in Figure 1.a. where we can observe that a 900 °C temperature is required to obtained a pure LTO phase. Under this temperature, we observe reflections peaks of the $LaTiO_3$ phase. The presence of this phase can be explained by the combustion of glycine, which induces a significant production of reducing gas, promoting the formation of Ti^{3+}. All observed X-ray reflections were indexed with $La_2Ti_2O_7$

layered-perovskite structure with $P2_1$ space group[38]. There is an evolution of the Full Width at Half Maximum (FWHM) that become narrow as the temperature increase, which is due to the coalescence of grains and the average crystallite size is calculated using Scherrer's relation[71,72] (Table 1).

We also know that $La_2Ti_2O_7$ is a n type semiconductor with a direct allowed transition, so we characterise the band gap of synthesized materials with UV-vis diffuse reflectance and using Tauc equation described in experimental part (Table 1). The optical band gap for LTO-AG synthesized between 800 and 1 100°C are very close around 4 eV (Figure 1.b). The shallower slope observed for LTO-AG-800 probably indicates the level of defect states (Urbach tail induced by a disorder)[76] greater in the case of a lower annealing temperature.

The specific surface area (S_{BET}) was calculated from adsorption isotherm by BET method and significantly decrease when the calcination temperature is lowered which confirm the coalescence of LTO grains and will have an antagonist effect impact on the photocatalytic efficiency. The average pore size was determined by BJH method and show an increase when temperature decrease due to coalescence of grain. Finally, we observe that the total pore volume (determined from the amount of nitrogen adsorbed at a relative pressure (P/P_0) of 0.95 in order not to consider the inter-particles porosity) decrease with temperature highlighting a decrease in the number of pores. All those results are summarised in Table 1. In this one, an increase of crystallites size can be observed with temperature, when this size increases the specific surface area (S_{BET}), the average pore size and the total porous volume decrease significantly. Note that the uncertainties compiled in table 1 were obtained from a standard deviation performed on a series of 3 independent measurements.

Table 1. Average crystallite size determined by XRD profile refinement, BET surface area, average pore size, total pore volume and optical band gap of the LTO-AG-X samples

Sample	Average crystallites size (nm)	S_{BET} ($m^2.g^{-1}$)	Average pore size (nm)	Total porous Volume ($cm^3.g^{-1}$)	E_g (eV)
LTO-AG-800	47 ± 4	10.6 ± 0.6	17 ± 0.85	$4.8x10^{-2} \pm 2.4x10^{-3}$	3.95 ± 0.02
LTO-AG-900	53 ± 4	6.7 ± 0.4	11 ± 0.55	$1.9x10^{-2} \pm 1.0x10^{-3}$	4.09 ± 0.02
LTO-AG-1000	70 ± 5	1.9 ± 0.2	7 ± 0.35	$4.8x10^{-3} \pm 2.4x10^{-4}$	4.04 ± 0.02
LTO-AG-1100	85 ± 6	0.6 ± 0.1	4 ± 0.20	$1.3x10^{-3} \pm 6.5x10^{-4}$	4.09 ± 0.02

The powder $La_2Ti_2O_7$ was studied by both TEM and SEM coupled with EDS analyses. SEM observations have shown a powder form the irregular agglomerates (Figure 2). Moreover, the observed lack of segregation clearly suggests the presence of chemically homogenous solution (Figure 2.b to 2.d) consistent with the identified $La_2Ti_2O_7$ phase what was confirmed by qualitative analysis EDS.

The morphology of $La_2Ti_2O_7$ (calcined at the temperature of 1000°C) grains with a corresponding electron diffraction pattern is presented in Figure 3. The grains have a diameter in the range 70-150 nm (Figure 3.a). The grain size observed in TEM is consistent with the crystallite size determined by XRD. The particle presented in Figure 3.b was identified as $La_2Ti_2O_7$ (monoclinic with *P2₁* space group). Experimental selected area electron diffraction (SAED) pattern taken from this particle showed a solution for [211] zone axis (Figure 3.c).

3.2. Photocatalytic Activity

3.2.1. Study on Rhodamine B

In order to quantify the efficiency of the photocatalyst, we carried out a study of the photodegradation of rhodamine B (C_0 = 4 $mg.L^{-1}$) by following the kinetics by UV-Visible

spectrometer based on the maximum adsorption of the dye (λ = 654 nm) and by Total Organic Carbon (TOC) Analysis. For this, a dispersion of 100 mg of photocatalyst was made in 200 mL aqueous solution of rhodamine B. All LTO-AG-X samples were studied, and the one synthesized at 1000°C exhibited the best photocatalytic properties with $k_{app} = 11.49x10^{-2}$ min^{-1} (Figure 4.a) i.e. a photodegradation rate of 50.1 $\mu mol.g_{cat}^{-1}.h^{-1}$. This sample will be considered for all others analysis. In the TOC analysis, we can observe that even if the discoloration of the solution is complete the mineralization step is not reach yet, because of the presence of degradation product of Rhodamine B. Thus, 90% of complete mineralization is obtained after 75 min (Figure 4.b).

In order to compare the photocatalytic efficiency between the synthetic routes (usual Sol-Gel (SG) method and Sol-Gel Assisted by Glycine (SG-AG)) with respect to the TiO_2 P25 Degussa®, the apparent rate constants were determined. For the SG method, an apparent rate constant of $1.79x10^{-2}$ min^{-1} was obtained (figure 4.c), this rate increases strongly in the case of the SG-AG method at $11.49x10^{-2}$ min^{-1} (more than six times greater). For comparison, this k_{app} is almost twice as high as the TiO_2 reference, whose value is $6.16x10^{-2}$ min^{-1}. This can be explained by the fact that the glycine has a surfactant role which allow a better dispersion of precursors in the gel and can react with the oxygen in air to create hot spots that leads to a massive gas release that limits the rise of temperature, avoid partial sintering of particles and generally allows to have a better specific surface area[77,78]. For the same calcination temperature of 1 000°C we observed for the Sol-Gel synthesis a specific surface area of 1 $m^2.g^{-1}$ [27] and for the assisted by glycine method a specific surface area which is nearly as double as the previous one (i.e. 1.9 $m^2.g^{-1}$). In addition, we can note the total pore volume increases slightly from $3.7x10^{-3}$ to $4.8x10^{-3}$ $cm^3.g^{-1}$ for the SG[27] and AG pathways (present work), respectively. The important difference is the drastic decrease in the average pore size from 36 nm to 7 nm for the SG and AG pathways, respectively. This increase in the number of pores

and the presence of straight channels may explain the increase in photocatalytic properties. B. Guo et *al.*[79] describes this behavior in mesoporous TiO_2 synthetized by sol-gel route using various surfactants.

Reaction intermediates have a negative role on the adsorption of the dye on the catalyst surface[80]. To study the influence of those intermediates two types of recyclability tests have been performed. In the first one, the solution was kept intact after a defined irradiation time (90 min) and Rhodamine B was then added to reach the same initial concentration before running another degradation test. In this one (Figure 4.d), we can observe a decrease of the percentage of discoloration at 90 min over 4 successive runs. In the second method particles were collected by centrifugation after 90 min and washed with water and ultrasounds without any thermic treatment. Then those particles were poured in a new batch with the same initial concentration of Rhodamine B and irradiate for another 90 min. For this second method, we can observe (Figure 4.d) that there is no decrease on the efficiency over 4 consecutives runs. We can conclude that the intermediate which are present in the solution before the mineralisation step can be adsorbed at the catalyst surface during photodegradation and reduce the efficiency of the catalyst on the dye degradation. It is also important to note that LTO-AG-X sample can be easily collected and remove from cleaned water by only centrifugation step, which means that this material can be recycling without complex treatment or procedure.

Initially, Rhodamine B was chosen as a model molecule in order to demonstrate the catalytic efficiency of the catalysts. Subsequently, phenol was chosen to continue our investigations given the fact that it is a toxic molecule present in many industrial wastewaters, the discharges of which are regulated. Indeed, this molecule is a very widespread pollutant in many industrial effluents from the petroleum[81], resin and paint fabrication[82,83], tannery[84] or even pharmaceutical industries[85]. For the drinking water, the World Health Organization advises a guideline concentration of phenol to 1 $\mu g.L^{-1}$ [86]. As the discharges are

regulated according to the standards of the countries, it is necessary to ensure the effluent before discharge into natural environments (general effluent discharge standard of phenol is 0.05 ppm[87]). The following paragraph aims to study the potential of the $La_2Ti_2O_7$ photocatalyst synthesized by glycine on the UV photodegradation of Phenol.

3.2.2. Study on Phenol

3.2.2.1. Influence of photocatalyst loading

The photodegradation of phenol have been monitored by UV-visible spectroscopic method based on the maximum adsorption of the compound (λ = 270 nm)[88]. In Figure 5.a, we can observe the evolution of the apparent rate constant for several photocatalyst loading (the initial concentration of phenol is fixed to 50 $mg.L^{-1}$). First, we can note a linear increase in the efficiency with the catalyst loading which has already been observed on other catalyst such as ZnO and TiO_2[89] and is due to the increase of available photocatalytic sites. An optimal loading of 0,5 $g.L^{-1}$ is obtained for the LTO-AG in the case of phenol degradation and the apparent rate constant corresponds to 5.5 $x10^{-3}$ min^{-1} i.e. a photodegradation rate of 47.0 $\mu mol.g_{cat}^{-1}.h^{-1}$. For higher loading we can observe an exponential decrease in the photocatalytic efficiency which can be due to several phenomena such as an increase in the agglomeration of particles or a screening effect that does not allow the light flux to deeply penetrate the solution and reach all photocatalyst particles.

3.2.2.2. Influence of irradiated surface

It is commonly admitted that photocatalytic degradation is proportional to the luminous flux receive[90,91]. Thus, the kinetic of the reaction is modified according to the following equation[92] :

$$v = v'\phi^n \qquad (5)$$

Where v' is the reaction rate independent of photon flux, Φ is the light density and the exponent n has a value between 0 and 1. Indeed, this n value can change from 1 for low flux to reach a value of ½ when the flux increases and 0 when the saturation is reached. For low intensities, the reaction rate is directly proportional to the light intensity. The electron-hole pairs are consumed and participate mainly in the chemical surface reaction. Beyond a certain limit value of luminous intensity, the dependence is carried out in square root. This evolution of n exponent probably results in a limitation of the charge transfer and a higher rate of recombination of the electron-hole pairs. Additionally, at even higher light intensity, a stationary state is reached, and the reaction rate saturates.

Several tests have then been made by using photoreactor with different diameter and the same loading of catalyst and light flux penetration. A linear evolution of the apparent rate constant as a function of irradiated surface can be observed in Figure 5.b. This evolution gives us some information on the fact that the saturation phenomenon has not been reached yet. Furthermore, the linear evolution also indicates that the photoreaction takes place close to the surface of the photoreactor because it is directly proportional to this one, which can be explained by an absorption of UV radiations by the aqueous solvent.

3.2.2.3 Influence of pH

In photocatalytic processes, the pH could have an influence on the properties of semiconductor catalyst such as it is charge surface or dissociation in the solution[93], but also on the species to be degraded and its adsorption[94]. The study on the zeta potential in LTO oxides have already been described in our previous work[27]. The Point of Zero Charge (PZC) is reached for a pH value of 8, under this pH lanthanum dititanate oxide particles are positively charged and above this they are negatively charged which would have an importance because

phenol can be observed under positively and negatively charged species depending on the pH of solution. Figure 5.c shows the influence of pH with and without catalyst on phenol.

This behavior is explained by the fact that phenol has two pK_a values which are: $pKa_1(PhOH_2^{+}/PhOH)$=-6.4 and $pKa_2(PhOH/PhO^{-})$=9.95 at 25°C [95]. Thus, for a pH greater than 9.95, the phenolate form is negatively charged. At pH = 12, as the surface of the photocatalyst is also negatively charged, the photocatalysis is disadvantaged. While at a pH below the PZC (i.e. pH = 8), photocatalysis is more favored (hence the best efficiency is observed at pH = 5.2 with $k_{app} = 5.49x10^{-3}$ min^{-1})). For more acidic pH, the efficiency decreases because the phenol is naturally degraded; thus at pH = 2 the degradation rates with and without photocatalyst are practically identical.This requirement of neutral condition has been already observed in literature for TiO_2 and $La_2Ti_2O_7$ compounds[93,96,97].

3.2.2.4 Comparison between $La_2Ti_2O_7$ and TiO_2

Figure 5.d shows the comparison of the degradation of phenol without catalyst and with catalyst TiO_2 P25 Degussa® and synthesized $La_2Ti_2O_7$. The influence of UV light alone on phenol can be observe with an apparent rate constant of $1.78x10^{-3}$ min^{-1}, for TiO_2 this constant is about $2.84x10^{-3}$ min^{-1} and for the AG method we obtained an apparent rate constant of $5.49x10^{-3}$ min^{-1}. This increase is similar as the one obtained on Rhodamine B and can be explained the same way. This similarity in the improvement of the photocatalytic properties seems to be independent of the nature of the species to be photodegraded showing that the material performance depends mainly upon microstructure, size, morphology of this oxide.

Some intermediates are still present in solution and can have a negative role on photodegradation In Figure 6, the variation of the total organic carbon can be observed. The half-time of the reaction is determined at 10 hours.

3.2.2.5 Influence of scavengers and photodegradation mechanism

During photocatalytic process various species are created such as holes and radicals[98–100] .In order to have a better understanding of which one have an influence on the photodegradation mechanism some tests have been made with scavenger species. Three species where used, the ethylenediaminetetraacetic acid (EDTA), the ascorbic acid and isopropanol to collect holes (h^+), superoxide radicals ($O_2^{\bullet -}$) and hydroxyl radicals ($HO^\bullet$), respectively. In Figure 6 no change has been observed in the apparent rate constant with the use of isopropanol which means the hydroxyl radicals don't have a role in photocatalytic process, the use of EDTA and ascorbic acid imply a variation of the apparent constant that decrease drastically which indicate that holes and superoxide radicals have an important role on the mechanism of degradation for $La_2Ti_2O_7$. The important role of superoxide radicals has already been observed for LTO[99,100].

3.2.3 Sonophotocatalysis

In sonophotocatalytic processes both UV irradiation and ultrasounds are used to improve the efficiency of photodegradation. UV light coupled with the catalyst will create hole/electron pair that will be used to decompose pollutants. Ultrasonic waves will create cavitation bubbles, when those previous one collapse they produce important energy and heat that leads in the formation of free radicals issued from the water[101,102]. The used of ultrasonic wave also allow a better dispersion of catalyst that increase the active surface reachable by the species to be degraded[103]. In order to study the influence of sonophotocatalysis the photoreactor containing 200 mL of aqueous solution of phenol with 0.5 $g.L^{-1}$ of catalyst has been placed in an ultrasonic bath (37 kHz) and result are shown in Figure 8.a. The apparent rate constant of photocatalysis (PC), sonocatalysis (SC) and

sonophotocatalysis (SPC) have been compared and are $3.21x10^{-3}$ min^{-1}, $5.74x10^{-4}$ min^{-1} and $3.58x10^{-3}$ min^{-1} respectively. A small increase can be observed with the use of both ultrasound and UV irradiation, it's also important to note that the volume of solution can have a role on ultrasonic waves effect. Indeed, if the volume in reactor decrease, the intensity of ultrasound increase that could lead to an even better dispersion and desorption of product on catalyst. In order to study the influence of volume three test have been made with the exact same condition (catalyst loading, concentration of phenol, light flux, …) and three different volume of 200, 100 and 50 mL. Figure 8.b shows this influence, and a better efficiency was obtained in sonophotocatalysis for a small volume with an apparent rate constant that goes from $3.58x10^{-3}$ min^{-1} for 200 mL to $6.43x10^{-3}$ min^{-1} for 50 mL.

4. Conclusion

La_2Ti_2O nanoparticles were successfully synthesized by a new Sol-Gel coupled to glycine combustion route. These nanoparticles were characterized by XRD, BET, SEM, EDS and TEM and we found that a minimal calcination temperature of 900°C is required to obtain the pure $La_2Ti_2O_7$ phase. The size of these particles was determined by using Scherrer's formula. The increase of crystallite size and the decrease of surface area with temperature was pointed out. Photodegradation tests have been made on Rhodamine B and phenol and shows a better photocatalytic efficiency for LTO-AG nanopowders synthesized at 1 000 °C. The experimental conditions such as catalyst loading and pH to obtain the better efficiency were determined. Total organic carbon measurements were carried out showing that there are intermediates present in solution before mineralisation step. We pointed out with recyclability tests that those intermediates have a counterproductive role on photodegradation. We investigate the role of radicals and holes produced on the mechanism of photodegradation with various scavenger's species and conclude that superoxide radicals and holes have the most

important role on the photodegradation. We also made sonophotocatalysis study and pointed out the influence of volume in the efficiency of ultrasound and the increase in sonophotocatalytic activity with the use of both ultrasound and UV irradiation.

Acknowledgments

The work was financially supported by « les Ministères de l'Europe et des Affaires Etrangères (MEAE) et de l'Enseignement Supérieur, de la Recherche et de l'Innovation (MESRI) » and the national agency for academic exchange of Poland (Narodowa Agencja Wymiany Akademickiej - NAWA) - PHC Polonium (N° 44701ZK). Chevreul Institute (FR 2638)", "Ministère de l'Enseignement Supérieur et de la Recherche", "Région Hauts-de-France", "FEDER" and "C'Nano Nord-Ouest compétence centre" are also acknowledged for supporting and funding this work.

Reference

[1] I.M. Arabatzis, T. Stergiopoulos, M.C. Bernard, D. Labou, S.G. Neophytides, P. Falaras, Silver-modified titanium dioxide thin films for efficient photodegradation of methyl orange, Appl. Catal. B Environ. 42 (2003) 187–201. https://doi.org/10.1016/S0926-3373(02)00233-3.

[2] M.J. Height, S.E. Pratsinis, O. Mekasuwandumrong, P. Praserthdam, Ag-ZnO catalysts for UV-photodegradation of methylene blue, Appl. Catal. B Environ. 63 (2006) 305–312. https://doi.org/10.1016/j.apcatb.2005.10.018.

[3] P. Wilhelm, D. Stephan, Photodegradation of rhodamine B in aqueous solution via SiO_2@TiO_2 nano-spheres, J. Photochem. Photobiol. Chem. 185 (2007) 19–25. https://doi.org/10.1016/j.jphotochem.2006.05.003.

[4] J. hui Sun, Y. kui Wang, R. xia Sun, S. ying Dong, Photodegradation of azo dye Congo Red from aqueous solution by the WO_3-TiO_2/activated carbon (AC) photocatalyst under the UV irradiation, Mater. Chem. Phys. 115 (2009) 303–308. https://doi.org/10.1016/j.matchemphys.2008.12.008.

[5] D. Awfa, M. Ateia, M. Fujii, M.S. Johnson, C. Yoshimura, Photodegradation of pharmaceuticals and personal care products in water treatment using carbonaceous-TiO_2 composites: A critical review of recent literature, Water Res. 142 (2018) 26–45. https://doi.org/10.1016/j.watres.2018.05.036.

[6] M. Thiruppathi, M. Vahini, P. Devendran, M. Arunpandian, K. Selvakumar, C. Ramalingan, M. Swaminathan, E.R. Nagarajan, $CuWO_4$ Nanoparticles: Investigation of Dielectric, Electrochemical Behaviour and Photodegradation of Pharmaceutical Waste , J. Nanosci. Nanotechnol. 19 (2019) 7026–7034. https://doi.org/10.1166/jnn.2019.16601.

[7] P. Stepnowski, E.M. Siedlecka, P. Behrend, B. Jastorff, Enhanced photo-degradation of contaminants in petroleum refinery wastewater, Water Res. 36 (2002) 2167–2172. https://doi.org/10.1016/S0043-1354(01)00450-X.

[8] D.C. Schmelling, K.A. Gray, Photocatalytic transformation and mineralization of 2,4,6-trinitrotoluene (TNT) in TiO_2 slurries, Water Res. 29 (1995) 2651–2662. https://doi.org/10.1016/0043-1354(95)00136-9.

[9] H.D. Burrows, M. Canle L, J.A. Santaballa, S. Steenken, Reaction pathways and mechanisms of photodegradation of pesticides, J. Photochem. Photobiol. B. 67 (2002) 71–108. https://doi.org/10.1016/S1011-1344(02)00277-4.

[10] N. Bustos, A. Cruz-Alcalde, A. Iriel, A. Fernández Cirelli, C. Sans, Sunlight and UVC-254 irradiation induced photodegradation of organophosphorus pesticide dichlorvos in aqueous matrices, Sci. Total Environ. 649 (2019) 592–600. https://doi.org/10.1016/j.scitotenv.2018.08.254.
[11] E. Yousif, R. Haddad, Photodegradation and photostabilization of polymers, especially polystyrene: Review, SpringerPlus. 2 (2013) 1–32. https://doi.org/10.1186/2193-1801-2-398.
[12] T.F. Yeh, J.M. Syu, C. Cheng, T.H. Chang, H. Teng, Graphite oxide as a photocatalyst for hydrogen production from water, Adv. Funct. Mater. 20 (2010) 2255–2262. https://doi.org/10.1002/adfm.201000274.
[13] X. Wang, K. Maeda, A. Thomas, K. Takanabe, G. Xin, J.M. Carlsson, K. Domen, M. Antonietti, A metal-free polymeric photocatalyst for hydrogen production from water under visible light, Nat. Mater. 8 (2009) 76–80. https://doi.org/10.1038/nmat2317.
[14] Q.L. Yang, S.Z. Kang, H. Chen, W. Bu, J. Mu, $La_2Ti_2O_7$: An efficient and stable photocatalyst for the photoreduction of Cr(VI) ions in water, Desalination. 266 (2011) 149–153. https://doi.org/10.1016/j.desal.2010.08.018.
[15] T. Alammar, A.V. Mudring, Facile preparation of Ag/ZnO nanoparticles via photoreduction, J. Mater. Sci. 44 (2009) 3218–3222. https://doi.org/10.1007/s10853-009-3429-4.
[16] V.K. Yemmireddy, Y.C. Hung, Using Photocatalyst Metal Oxides as Antimicrobial Surface Coatings to Ensure Food Safety—Opportunities and Challenges, Compr. Rev. Food Sci. Food Saf. 16 (2017) 617–631. https://doi.org/10.1111/1541-4337.12267.
[17] C.A. Emilio, M.I. Litter, M. Kunst, M. Bouchard, C. Colbeau-Justin, Phenol photodegradation on platinized-TiO_2 photocatalysts related to charge-carrier dynamics, Langmuir. 22 (2006) 3606–3613. https://doi.org/10.1021/la051962s.
[18] P. Sawunyama, A. Fujishima, K. Hashimoto, Photocatalysis on TiO_2 surfaces investigated by atomic force microscopy: photodegradation of partial and full monolayers of stearic acid on TiO_2(110), Langmuir. 15 (1999) 3551–3556. https://doi.org/10.1021/la9814440.
[19] Y.H. Hsien, C.F. Chang, Y.H. Chen, S. Cheng, Photodegradation of aromatic pollutants in water over TiO_2 supported on molecular sieves, Appl. Catal. B Environ. 31 (2001) 241–249. https://doi.org/10.1016/S0926-3373(00)00283-6.
[20] J. Schneider, M. Matsuoka, M. Takeuchi, J. Zhang, Y. Horiuchi, M. Anpo, D.W. Bahnemann, Schneider et al. - 2014 - Understanding TiO_2 Photocatalysis Mechanisms and Materials(2).pdf, Chem Rev. 114 (2014) 9919−9986.
[21] A. Bhattacharjee, M. Ahmaruzzaman, T. Sinha, A novel approach for the synthesis of SnO_2 nanoparticles and its application as a catalyst in the reduction and photodegradation of organic compounds, Spectrochim. Acta - Part Mol. Biomol. Spectrosc. 136 (2015) 751–760. https://doi.org/10.1016/j.saa.2014.09.092.
[22] Y.C. Liang, C.W. Chang, Preparation of orthorhombic WO_3 thin films and their crystal quality-dependent dye photodegradation ability, Coatings. 9 (2019). https://doi.org/10.3390/COATINGS9020090.
[23] M. El-Kemary, H. El-Shamy, Fluorescence modulation and photodegradation characteristics of safranin O dye in the presence of ZnS nanoparticles, J. Photochem. Photobiol. Chem. 205 (2009) 151–155. https://doi.org/10.1016/j.jphotochem.2009.04.021.
[24] A. Malathi, J. Madhavan, M. Ashokkumar, P. Arunachalam, A review on $BiVO_4$ photocatalyst: Activity enhancement methods for solar photocatalytic applications, Appl. Catal. Gen. 555 (2018) 47–74. https://doi.org/10.1016/j.apcata.2018.02.010.
[25] C. Pan, J. Xu, Y. Chen, Y. Zhu, Influence of OH-related defects on the performances of $BiPO_4$ photocatalyst for the degradation of rhodamine B, Appl. Catal. B Environ. 115–116 (2012) 314–319. https://doi.org/10.1016/j.apcatb.2011.12.030.
[26] H. Wang, L. Du, L. Yang, W. Zhang, H. He, Sol-gel synthesis of $La_2Ti_2O_7$ modified with PEG4000 for the enhanced photocatalytic activity, J. Adv. Oxid. Technol. 19 (2016) 366–371. https://doi.org/10.1515/jaots-2016-0221.
[27] S. Leroy, J.F. Blach, M. Huvé, B. Léger, N. Kania, J.F. Henninot, A. Ponchel, S. Saitzek, Photocatalytic and sonophotocatalytic degradation of rhodamine B by nano-sized $La_2Ti_2O_7$ oxides synthesized with sol-gel method, J. Photochem. Photobiol. Chem. 401 (2020) 112767. https://doi.org/10.1016/j.jphotochem.2020.112767.
[28] A.M. Smith, S. Nie, Semiconductor nanocrystals: Structure, properties, and band gap engineering, Acc. Chem. Res. 43 (2010) 190–200. https://doi.org/10.1021/ar9001069.
[29] W.J. Yin, S. Chen, J.H. Yang, X.G. Gong, Y. Yan, S.H. Wei, Effective band gap narrowing of anatase TiO_2 by strain along a soft crystal direction, Appl. Phys. Lett. 96 (2010). https://doi.org/10.1063/1.3430005.
[30] M. Ahmed, G. Xinxin, A review of metal oxynitrides for photocatalysis, Inorg. Chem. Front. 3 (2016) 578–590. https://doi.org/10.1039/c5qi00202h.
[31] R. Kuriki, T. Ichibha, K. Hongo, D. Lu, R. Maezono, H. Kageyama, O. Ishitani, K. Oka, K. Maeda, A Stable, Narrow-Gap Oxyfluoride Photocatalyst for Visible-Light Hydrogen Evolution and Carbon Dioxide Reduction, J. Am. Chem. Soc. 140 (2018) 6648–6655. https://doi.org/10.1021/jacs.8b02822.

[32] M. Zhu, X. Cai, M. Fujitsuka, J. Zhang, T. Majima, Au/$La_2Ti_2O_7$Nanostructures Sensitized with Black Phosphorus for Plasmon-Enhanced Photocatalytic Hydrogen Production in Visible and Near-Infrared Light, Angew. Chem. - Int. Ed. 56 (2017) 2064–2068. https://doi.org/10.1002/anie.201612315.
[33] N. Soltani, E. Saion, W.M.M. Yunus, M. Erfani, M. Navasery, G. Bahmanrokh, K. Rezaee, Enhancement of visible light photocatalytic activity of ZnS and CdS nanoparticles based on organic and inorganic coating, Appl. Surf. Sci. 290 (2014) 440–447. https://doi.org/10.1016/j.apsusc.2013.11.104.
[34] X. Zhou, T. Ju, Q. Wang, Synthesis of visible-light-driven g-C_3N_4/$La_2Ti_2O_7$ heterojunction photocatalysts for improved photocatalytic performance, J. Mater. Sci. Mater. Electron. 31 (2020) 1265–1274. https://doi.org/10.1007/s10854-019-02638-6.
[35] Y. Ao, K. Wang, P. Wang, C. Wang, J. Hou, Fabrication of novel p-n heterojunction BiOI/$La_2Ti_2O_7$ composite photocatalysts for enhanced photocatalytic performance under visible light irradiation, Dalton Trans. 45 (2016) 7986–7997. https://doi.org/10.1039/c6dt00862c.
[36] J. Chen, S. Liu, L. Zhang, N. Chen, New SnS_2/$La_2Ti_2O_7$ heterojunction photocatalyst with enhanced visible-light activity, Mater. Lett. 150 (2015) 44–47. https://doi.org/10.1016/j.matlet.2015.02.134.
[37] M. Kimura, S. Nanamatsu, K. Doi, S. Matsushita, M. Takahashi, Electrooptic and Piezoelectric Properties of La2Ti2O7 Single Crystal, Jpn. J. Appl. Phys. Part 1 Regul. Pap. Short Notes Rev. Pap. 11 (1972) 904. https://doi.org/10.1143/JJAP.11.904.
[38] M. Gasperin, Dititanate de lanthane, Acta Crystallogr. B. 31 (1975) 2129–2130. https://doi.org/10.1107/s0567740875007005.
[39] N. Ishizawa, F. Marumo, S. Iwai, M. Kimura, T. Kawamura, Compounds with perovskite-type slabs. V. A high-temperature modification of $La_2Ti_2O_7$, Acta Crystallogr. B. 38 (1982) 368–372. https://doi.org/10.1107/s0567740882002994.
[40] H. Yan, H. Ning, Y. Kan, P. Wang, M.J. Reece, Piezoelectric ceramics with super-high curie points, J. Am. Ceram. Soc. 92 (2009) 2270–2275. https://doi.org/10.1111/j.1551-2916.2009.03209.x.
[41] S. Nanamatsu, M. Kimura, K. Doi, S. Matsushita, N. Yamada, A new ferroelectric: $La_2Ti_2O_7$, Ferroelectrics. 8 (1973) 511–513. https://doi.org/10.1080/00150197408234143.
[42] A. Sayir, S.C. Farmer, F. Dynys, High Temperature Piezoelectric $La_2Ti_2O_7$, (2012) 57–68. https://doi.org/10.1002/9781118407899.ch6.
[43] P.B., R.M. P.T. Diallo, nti-Stokes luminescence and site selectivity in $La_2Ti_2O_7$:Pr^{3+}, J. Alloys Compd. 341 (2002) 139–143.
[44] H. Zhang, G. Li, Y. Zhu, S. Liu, K. Li, Y. Liang, Color tuning and white light emission in a single-phased $La_2Ti_2O_7$:Pr^{3+}, Tb^{3+} phosphor, J. Alloys Compd. 798 (2019) 800–809. https://doi.org/10.1016/j.jallcom.2019.05.306.
[45] J.Y. Park, S.J. Park, M. Kwak, H.K. Yang, Rapid visualization of latent fingerprints with Eu-doped $La_2Ti_2O_7$, J. Lumin. 201 (2018) 275–283. https://doi.org/10.1016/j.jlumin.2018.04.012.
[46] F. Szczepanski, A. Bayart, A. Katelnikovas, J.F. Blach, J. Rousseau, S. Saitzek, Luminescence and up-conversion properties in $La_2Ti_2O_7$:Eu^{3+},Er^{3+} oxides under UV and NIR radiations towards a two-color sensor, J. Alloys Compd. 826 (2020). https://doi.org/10.1016/j.jallcom.2020.154157.
[47] Z. Shao, S. Saitzek, J.-F. Blach, A. Sayede, P. Roussel, R. Desfeux, Structural Characterization and Photoluminescent Properties of $(La_{1-x}Sm_x)_2Ti_2O_7$ Solid Solutions Synthesized by a Sol-Gel Route, Eur. J. Inorg. Chem. 2011 (2011) 3569–3576. https://doi.org/10.1002/ejic.201100309.
[48] G. Lakshminarayana, R. Yang, M. Mao, J. Qiu, I. V. Kityk, Photoluminescence of Sm^{3+}, Dy^{3+}, and Tm^{3+}-doped transparent glass ceramics containing CaF_2 nanocrystals, J. Non-Cryst. Solids. 355 (2009) 2668–2673. https://doi.org/10.1016/j.jnoncrysol.2009.08.029.
[49] W.G.J.H.M. van Sark, J. de Wild, J.K. Rath, A. Meijerink, R.E.I. Schropp, Upconversion in solar cells, Nanoscale Res. Lett. 8 (2013) 81. https://doi.org/10.1186/1556-276X-8-81.
[50] T.F. Schulze, Y.Y. Cheng, B. Fückel, R.W. MacQueen, A. Danos, N.J.L.K. Davis, M.J.Y. Tayebjee, T. Khoury, R.G.C.R. Clady, N.J. Ekins-Daukes, M.J. Crossley, B. Stannowski, K. Lips, T.W. Schmidt, Photochemical Upconversion Enhanced Solar Cells: Effect of a Back Reflector, Aust. J. Chem. 65 (2012) 480. https://doi.org/10.1071/CH12117.
[51] M. Sun, L. Xu, W. Ma, X. Wu, H. Kuang, L. Wang, C. Xu, Hierarchical Plasmonic Nanorods and Upconversion Core-Satellite Nanoassemblies for Multimodal Imaging-Guided Combination Phototherapy, Adv. Mater. 28 (2016) 898–904. https://doi.org/10.1002/adma.201505023.
[52] R. Meenambal, S. Kannan, Cosubstitution of Lanthanides (Gd^{3+}/Dy^{3+}/Yb^{3+}) in β-$Ca_3(PO_4)_2$ for Upconversion Luminescence, CT/MRI Multimodal Imaging, ACS Biomater. Sci. Eng. 4 (2018) 47–56. https://doi.org/10.1021/acsbiomaterials.7b00742.
[53] J. Kim, D.W. Hwang, S.W. Bae, Effect of Precursors on the Morphology and the Photocatalytic Water-Splitting Activity of Layered Perovskite $La_2Ti_2O_7$, 18 (2001) 7.

[54] Q. Wang, T. Hisatomi, Y. Moriya, K. Maeda, K. Domen, Physicochemical properties and photocatalytic H2 evolution activity of Rh-doped $La_2Ti_2O_7$ prepared by molten salt synthesis, Catal. Sci. Technol. 3 (2013) 2098–2103. https://doi.org/10.1039/C3CY00179B.
[55] S. Hu, L. Jia, B. Chi, J. Pu, L. Jian, Visible light driven (Fe, Cr)-codoped $La_2Ti_2O_7$ photocatalyst for efficient photocatalytic hydrogen production, J. Power Sources. 266 (2014) 304–312. https://doi.org/10.1016/j.jpowsour.2014.05.054.
[56] D.W. Hwang, K.Y. Cha, J. Kim, H.G. Kim, S.W. Bae, J.S. Lee, Photocatalytic Degradation of CH_3Cl over a Nickel-Loaded Layered Perovskite, Ind. Eng. Chem. Res. 42 (2003) 1184–1189. https://doi.org/10.1021/ie020457c.
[57] D.W. Hwang, H.G. Kim, J.S. Jang, S.W. Bae, S.M. Ji, J.S. Lee, Photocatalytic decomposition of water–methanol solution over metal-doped layered perovskites under visible light irradiation, Catal. Today. 93–95 (2004) 845–850. https://doi.org/10.1016/j.cattod.2004.06.084.
[58] W.-M. Hou, Y. Ku, Synthesis and characterization of $La_2Ti_2O_7$ employed for photocatalytic degradation of reactive red 22 dyestuff in aqueous solution, J. Alloys Compd. 509 (2011) 5913–5918. https://doi.org/10.1016/j.jallcom.2011.03.042.
[59] W. Zhang, Z. Ma, L. Du, L. Yang, X. Chen, H. He, Effects of calcination temperature on characterization and photocatalytic activity of $La_2Ti_2O_7$ supported on HZSM-5 zeolite, J. Alloys Compd. 695 (2017) 3541–3546. https://doi.org/10.1016/j.jallcom.2016.11.416.
[60] W. Zhang, H. Li, Z. Ma, H. Li, H. Wang, Photocatalytic degradation of azophloxine on porous $La_2Ti_2O_7$ prepared by sol-gel method, Solid State Sci. 87 (2019) 58–63. https://doi.org/10.1016/j.solidstatesciences.2018.11.004.
[61] H. Wang, Y. Zhang, Z. Ma, W. Zhang, Role of PEG2000 on sol-gel preparation of porous $La_2Ti_2O_7$ for enhanced photocatalytic activity on ofloxacin degradation, Mater. Sci. Semicond. Process. 91 (2019) 151–158. https://doi.org/10.1016/j.mssp.2018.11.025.
[62] Y. Ku, L.-C. Wang, C.-M. Ma, Photocatalytic Oxidation of Isopropanol in Aqueous Solution Using Perovskite-Structured $La_2Ti_2O_7$, Chem. Eng. Technol. 30 (2007) 895–900. https://doi.org/10.1002/ceat.200700071.
[63] M. Salavati-Niasari, F. Davar, Z. Fereshteh, Synthesis of nickel and nickel oxide nanoparticles via heat-treatment of simple octanoate precursor, J. Alloys Compd. 494 (2010) 410–414. https://doi.org/10.1016/j.jallcom.2010.01.063.
[64] S. Ahmadian-Fard-Fini, M. Salavati-Niasari, D. Ghanbari, Hydrothermal green synthesis of magnetic Fe_3O_4-carbon dots by lemon and grape fruit extracts and as a photoluminescence sensor for detecting of E. coli bacteria, Spectrochim. Acta. A. Mol. Biomol. Spectrosc. 203 (2018) 481–493. https://doi.org/10.1016/j.saa.2018.06.021.
[65] K. Li, Y. Wang, H. Wang, M. Zhu, H. Yan, Hydrothermal synthesis and photocatalytic properties of layered $La_2Ti_2O_7$ nanosheets, Nanotechnology. 17 (2006) 4863–4867. https://doi.org/10.1088/0957-4484/17/19/014.
[66] H.G. Kim, D.W. Hwang, S.W. Bae, J.H. Jung, J.S. Lee, Photocatalytic Water Splitting over $La_2Ti_2O_7$ Synthesized by the Polymerizable Complex Method, Catal. Lett. 91 (2003) 193–198. https://doi.org/10.1023/B:CATL.0000007154.30343.23.
[67] Y. Zhou, Z. Mei, H. Ye, W. Su, X. Zhao, P. Tang, Preparation and Characterization of Nanocrystalline $La_2Ti_2O_7$ by Microwave Assisted Process, Mater. Sci. Forum. 852 (2016) 525–529. https://doi.org/10.4028/www.scientific.net/MSF.852.525.
[68] Z. Huang, J. Liu, L. Huang, L. Tian, Sen Wang, G. Zhang, J. Li, F. Liang, H. Zhang, Q. Jia, S. Zhang, One-step synthesis of dandelion-like lanthanum titanate nanostructures for enhanced photocatalytic performance, NPG Asia Mater. 12 (2020) 11. https://doi.org/10.1038/s41427-019-0194-y.
[69] Y. Xie, D. Kocaefe, C. Chen, Y. Kocaefe, Review of Research on Template Methods in Preparation of Nanomaterials, J. Nanomater. 2016 (2016) e2302595. https://doi.org/10.1155/2016/2302595.
[70] M. Salavati-Niasari, Nanoscale microreactor-encapsulation 14-membered nickel(II) hexamethyl tetraaza: synthesis, characterization and catalytic activity, J. Mol. Catal. Chem. 229 (2005) 159–164. https://doi.org/10.1016/j.molcata.2004.11.016.
[71] A. Cenovar, P. Paunovic, A. Grozdanov, P. Makreski, E. Fidancevska, Preparation of Nano-Crystalline TiO2 by Sol-Gel Method using Titanium Tetraisopropoxide (TTIP) as a Precursor, Adv. Nat. Sci. Theory Appl. 1 (2012) 133–142.
[72] A.J. Ying, C.E. Murray, I.C. Noyan, A rigorous comparison of X-ray diffraction thickness measurement techniques using silicon-on-insulator thin films, J. Appl. Crystallogr. 42 (2009) 401–410. https://doi.org/10.1107/S0021889809006888.
[73] J. Tauc, Optical properties and electronic structure of amorphous germanium, Phys. Status Solidi. (1966).

[74] A.B. Murphy, Band-gap determination from diffuse reflectance measurements of semiconductor films, and application to photoelectrochemical water-splitting, Sol. Energy Mater. Sol. Cells. 91 (2007) 1326–1337. https://doi.org/10.1016/j.solmat.2007.05.005.
[75] M. Rahimi-Nasrabadi, S. Mahdavi, K. Adib, Photocatalytically active $La_2Ti_2O_7$ nanostructures, synthesis and characterization, J. Mater. Sci. Mater. Electron. 28 (2017). https://doi.org/10.1007/s10854-017-7080-6.
[76] V.R. Akshay, B. Arun, G. Mandal, M. Vasundhara, Visible range optical absorption, Urbach energy estimation and paramagnetic response in Cr-doped TiO_2 nanocrystals derived by a sol-gel method, Phys. Chem. Chem. Phys. 21 (2019) 12991–13004. https://doi.org/10.1039/c9cp01351b.
[77] S.M. Khetre, H. V. Jadhav, S.R. Bamane, Synthesis and characterization of nanocrystalline $LaCrO_3$ by combustion route, Rasayan J. Chem. 2 (2009) 174–178.
[78] R.D. Purohit, B.P. Sharma, K.T. Pillai, A.K. Tyagi, Ultrafine ceria powders via glycine-nitrate combustion, Mater. Res. Bull. 36 (2001) 2711–2721. https://doi.org/10.1016/S0025-5408(01)00762-0.
[79] B. Guo, H. Shen, K. Shu, Y. Zeng, W. Ning, The study of the relationship between pore structure and photocatalysis of mesoporous TiO_2, J. Chem. Sci. 121 (2009) 317–321. https://doi.org/10.1007/s12039-009-0036-5.
[80] J. Matos, J. Laine, J.M. Herrmann, D. Uzcategui, J.L. Brito, Influence of activated carbon upon titania on aqueous photocatalytic consecutive runs of phenol photodegradation, Appl. Catal. B Environ. 70 (2007) 461–469. https://doi.org/10.1016/j.apcatb.2005.10.040.
[81] B.H. Diya'Uddeen, W.M.A.W. Daud, A.R. Abdul Aziz, Treatment technologies for petroleum refinery effluents: A review, Process Saf. Environ. Prot. 89 (2011) 95–105. https://doi.org/10.1016/j.psep.2010.11.003.
[82] C.C. Wang, C.Y. Chen, C.Y. Chang, Synthesis of chelating resins with iminodiacetic acid and its wastewater treatment application, J. Appl. Polym. Sci. 84 (2002) 1353–1362. https://doi.org/10.1002/app.10243.
[83] G.K. Latinwo, S.E. Agarry, B. Engineering, C.E. Biotechnology, Removal of Phenol from Paint Wastewater by Adsorption onto Phosphoric Acid Activated Carbon Produced from Coconut Shell : Isothermal and Kinetic Modelling Studies, 7 (2015) 123–138.
[84] R.N. Bharagava, G. Saxena, S.I. Mulla, D.K. Patel, Characterization and Identification of Recalcitrant Organic Pollutants (ROPs) in Tannery Wastewater and Its Phytotoxicity Evaluation for Environmental Safety, Arch. Environ. Contam. Toxicol. 75 (2018) 259–272. https://doi.org/10.1007/s00244-017-0490-x.
[85] M. Shourian, K.A. Noghabi, H.S. Zahiri, T. Bagheri, G. Karballaei, M. Mollaei, I. Rad, S. Ahadi, J. Raheb, H. Abbasi, Efficient phenol degradation by a newly characterized Pseudomonas sp. SA01 isolated from pharmaceutical wastewaters, Desalination. 246 (2009) 577–594. https://doi.org/10.1016/j.desal.2008.07.015.
[86] J. Yan, W. Jianping, B. Jing, W. Daoquan, H. Zongding, Phenol biodegradation by the yeast Candida tropicalis in the presence of m-cresol, Biochem. Eng. J. 29 (2006) 227–234. https://doi.org/10.1016/j.bej.2005.12.002.
[87] S. Aoudj, A. Khelifa, N. Drouiche, R. Belkada, D. Miroud, Simultaneous removal of chromium(VI) and fluoride by electrocoagulation-electroflotation: Application of a hybrid Fe-Al anode, Chem. Eng. J. 267 (2015) 153–162. https://doi.org/10.1016/j.cej.2014.12.081.
[88] B. Roig, C. Gonzalez, O. Thomas, Monitoring of phenol photodegradation by ultraviolet spectroscopy, Spectrochim. Acta - Part Mol. Biomol. Spectrosc. 59 (2003) 303–307. https://doi.org/10.1016/S1386-1425(02)00172-5.
[89] S. Sakthivel, B. Neppolian, M. V. Shankar, B. Arabindoo, M. Palanichamy, V. Murugesan, Solar photocatalytic degradation of azo dye: Comparison of photocatalytic efficiency of ZnO and TiO_2, Sol. Energy Mater. Sol. Cells. 77 (2003) 65–82. https://doi.org/10.1016/S0927-0248(02)00255-6.
[90] J.M. Herrmann, Heterogeneous photocatalysis: Fundamentals and applications to the removal of various types of aqueous pollutants, Catal. Today. 53 (1999) 115–129. https://doi.org/10.1016/S0920-5861(99)00107-8.
[91] D.F. Ollis, E. Pelizzetti, N. Serpone, Destruction of water contaminants, Environ. Sci. Technol. 25 (1991) 1522–1529. https://doi.org/10.1021/es00021a001.
[92] S.B. Kim, S.C. Hong, Kinetic study for photocatalytic degradation of volatile organic compounds in air using thin film TiO_2 photocatalyst, Appl. Catal. B Environ. 35 (2002) 305–315. https://doi.org/10.1016/S0926-3373(01)00274-0.
[93] C.H. Chiou, C.Y. Wu, R.S. Juang, Influence of operating parameters on photocatalytic degradation of phenol in UV/TiO_2 process, Chem. Eng. J. 139 (2008) 322–329. https://doi.org/10.1016/j.cej.2007.08.002.
[94] F. Azeez, E. Al-Hetlani, M. Arafa, Y. Abdelmonem, A.A. Nazeer, M.O. Amin, M. Madkour, The effect of surface charge on photocatalytic degradation of methylene blue dye using chargeable titania nanoparticles, Sci. Rep. 8 (2018) 1–9. https://doi.org/10.1038/s41598-018-25673-5.

[95] M.T. Combs, M. Ashraf-Khorassani, L.T. Taylor, pH effects on the direct supercritical fluid extraction of phenols from aqueous matrices, J. Supercrit. Fluids. 9 (1996) 122–127. https://doi.org/10.1016/S0896-8446(96)90008-X.
[96] Z.H. Yuan, J.H. Jia, L. De Zhang, Influence of co-doping of Zn(II) + Fe(III) on the photocatalytic activity of TiO2 for phenol degradation, Mater. Chem. Phys. 73 (2002) 323–326. https://doi.org/10.1016/S0254-0584(01)00373-X.
[97] M. Trillas, M. Pujol, X. Domènech, Phenol photodegradation over titanium dioxide, J. Chem. Technol. Biotechnol. 55 (1992) 85–90. https://doi.org/10.1002/jctb.280550114.
[98] T. Scott, H. Zhao, W. Deng, X. Feng, Y. Li, Photocatalytic degradation of phenol in water under simulated sunlight by an ultrathin MgO coated Ag/TiO_2 nanocomposite, Chemosphere. 216 (2019) 1–8. https://doi.org/10.1016/j.chemosphere.2018.10.083.
[99] F. Wang, S. Gu, R. Shang, P. Jing, Y. Wang, W. Li, Fabrication of AgBr/$La_2Ti_2O_7$ hierarchical heterojunctions: Boosted interfacial charge transfer and high efficiency visible-light photocatalytic activity, Sep. Purif. Technol. 229 (2019) 115798. https://doi.org/10.1016/j.seppur.2019.115798.
[100] S. Wan, F. Qi, W. Jin, X. Guo, H. Liu, J. Zhao, J. Zhang, C. Tang, Construction of ultrafine Ag_3PO_4 nanoparticle and $La_2Ti_2O_7$ nanosheet 0D/2D heterojunctions with improved photocatalytic performance, J. Alloys Compd. 740 (2018) 901–909. https://doi.org/10.1016/j.jallcom.2018.01.094.
[101] C.G. Joseph, G. Li Puma, A. Bono, D. Krishnaiah, Sonophotocatalysis in advanced oxidation process: A short review, Ultrason. Sonochem. 16 (2009) 583–589. https://doi.org/10.1016/j.ultsonch.2009.02.002.
[102] Y.G. Adewuyi, Sonochemistry: Environmental science and engineering applications, Ind. Eng. Chem. Res. 40 (2001) 4681–4715. https://doi.org/10.1021/ie010096l.
[103] D. Panda, S. Manickam, Recent advancements in the sonophotocatalysis (SPC) and doped-sonophotocatalysis (DSPC) for the treatment of recalcitrant hazardous organic water pollutants, Ultrason. Sonochem. 36 (2017) 481–496. https://doi.org/10.1016/j.ultsonch.2016.12.022.

Figure captions:

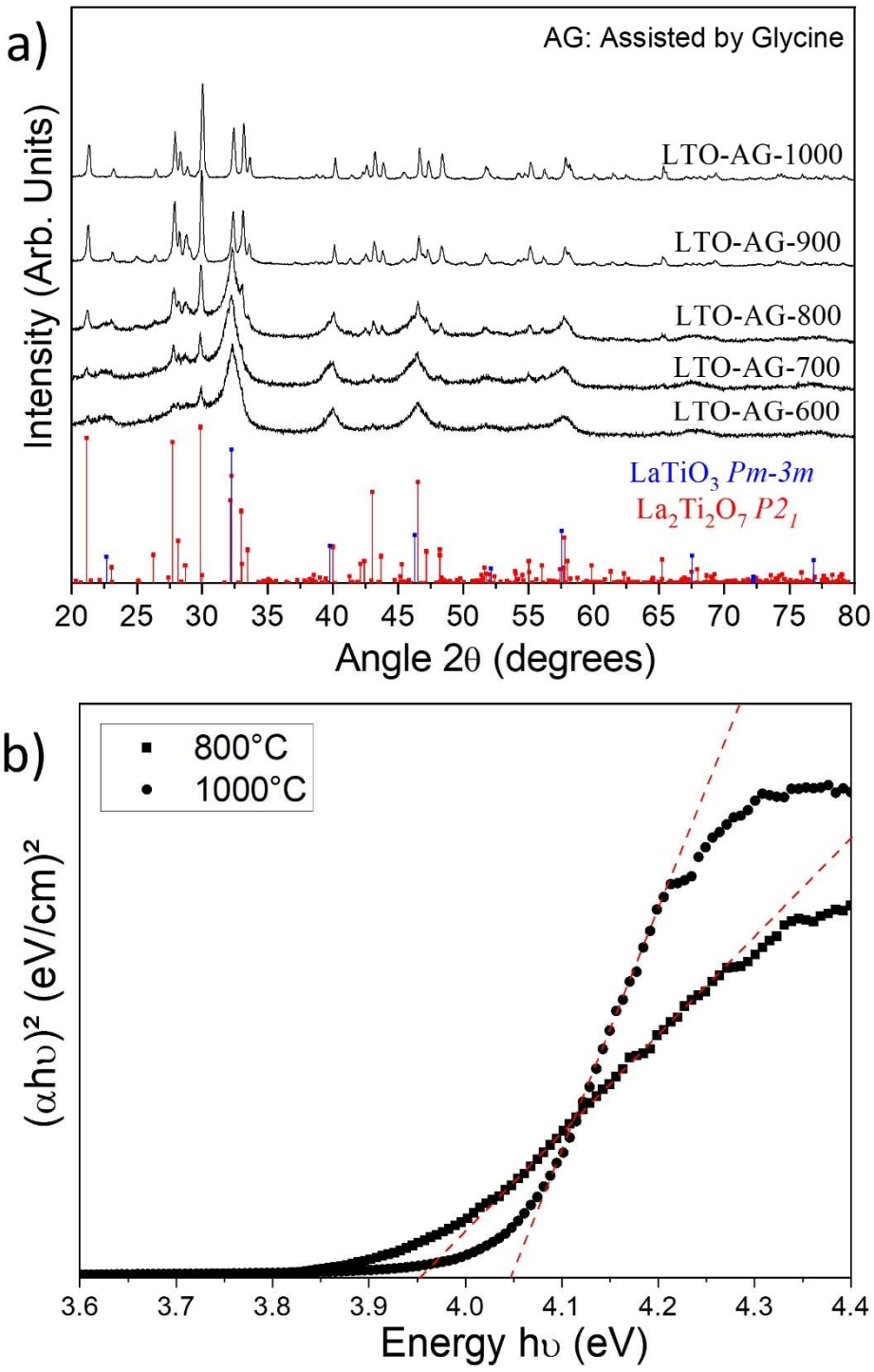

Figure 1.a) XRD patterns of LTO-AG obtained using different calcination temperature during synthesis and b) Tauc Plots of LTO-AG-800 and LTO-AG-1000.

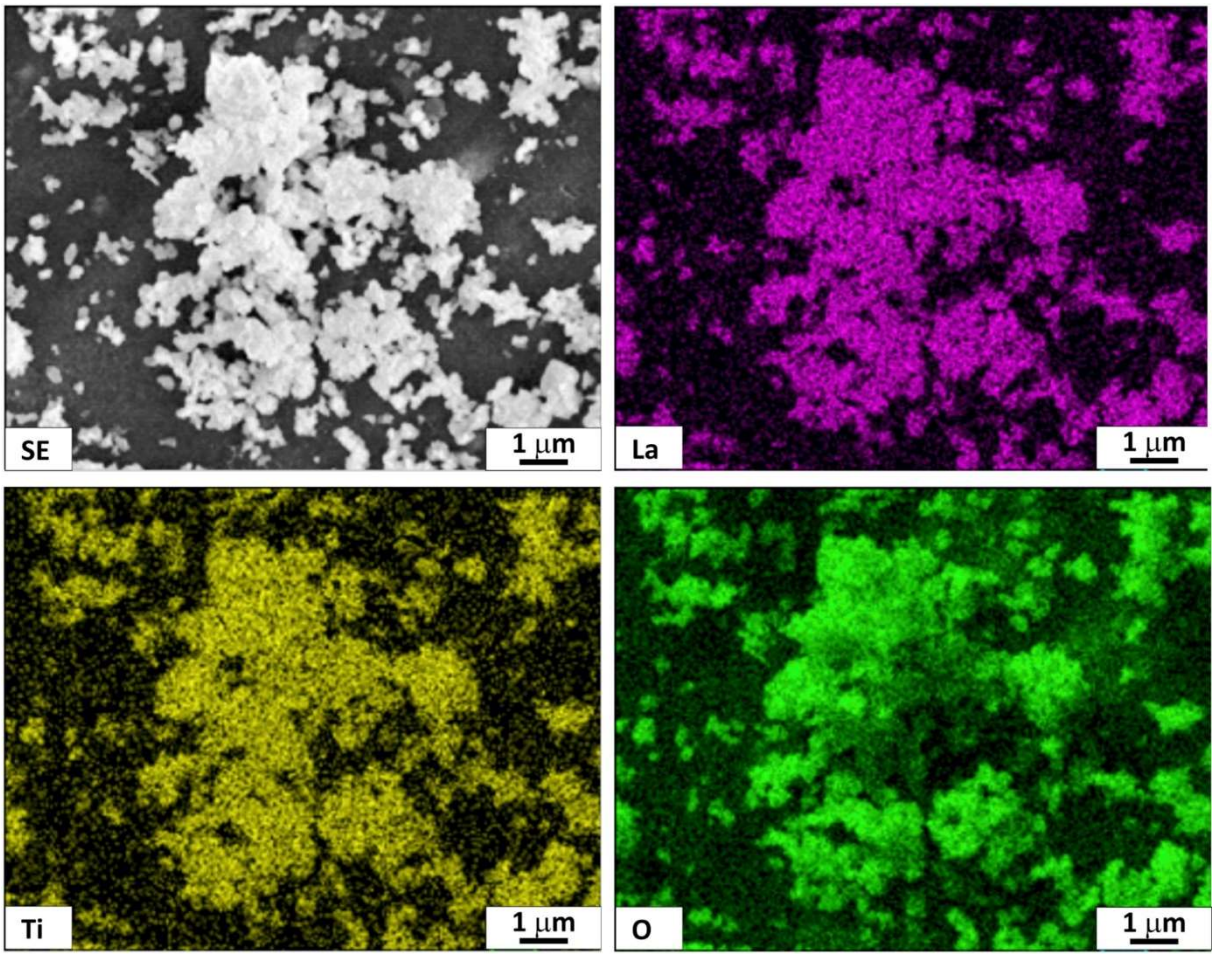

Figure 2. SEM image of $La_2Ti_2O_7$ powder with EDS elements distribution for La, Ti and O.

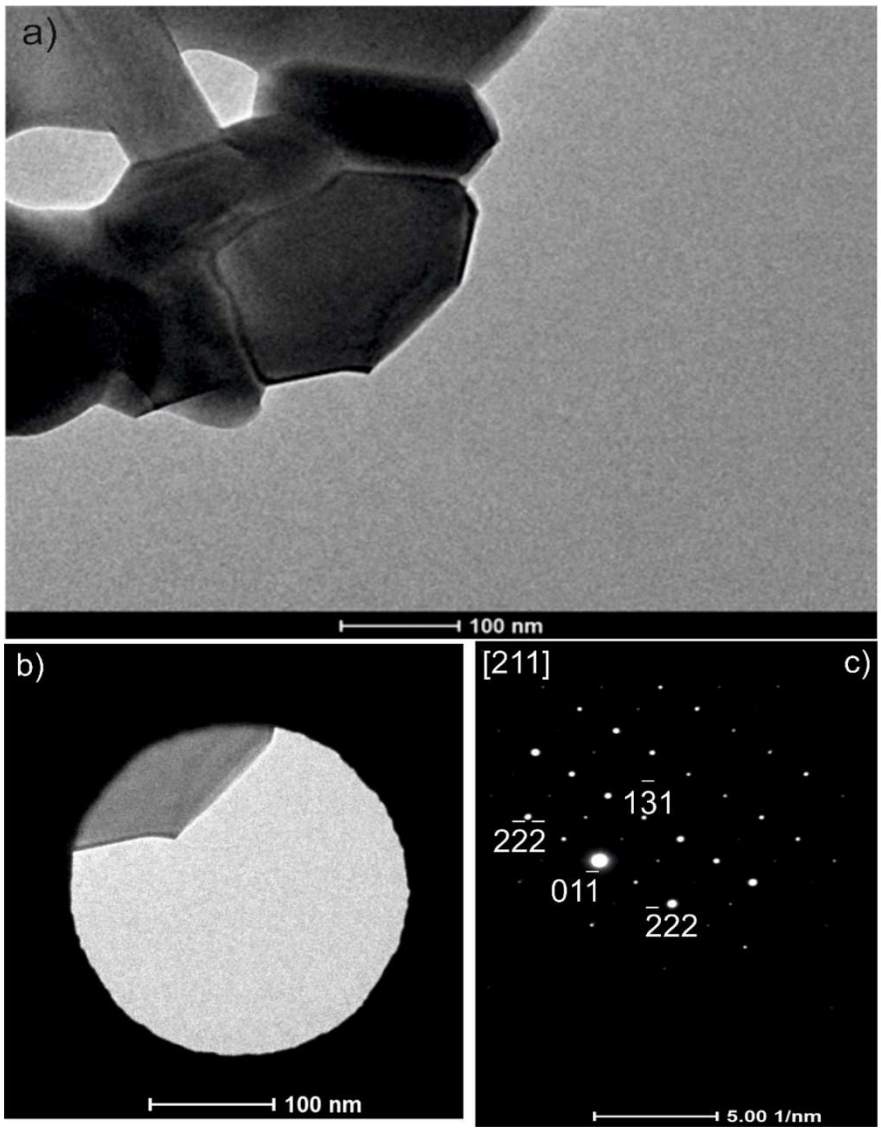

Figure 3. Microphotograph transmission electron microscopy a) particles of LTO-AG-1000 b) part of grain c) diffraction pattern with solution for [211] zone axis.

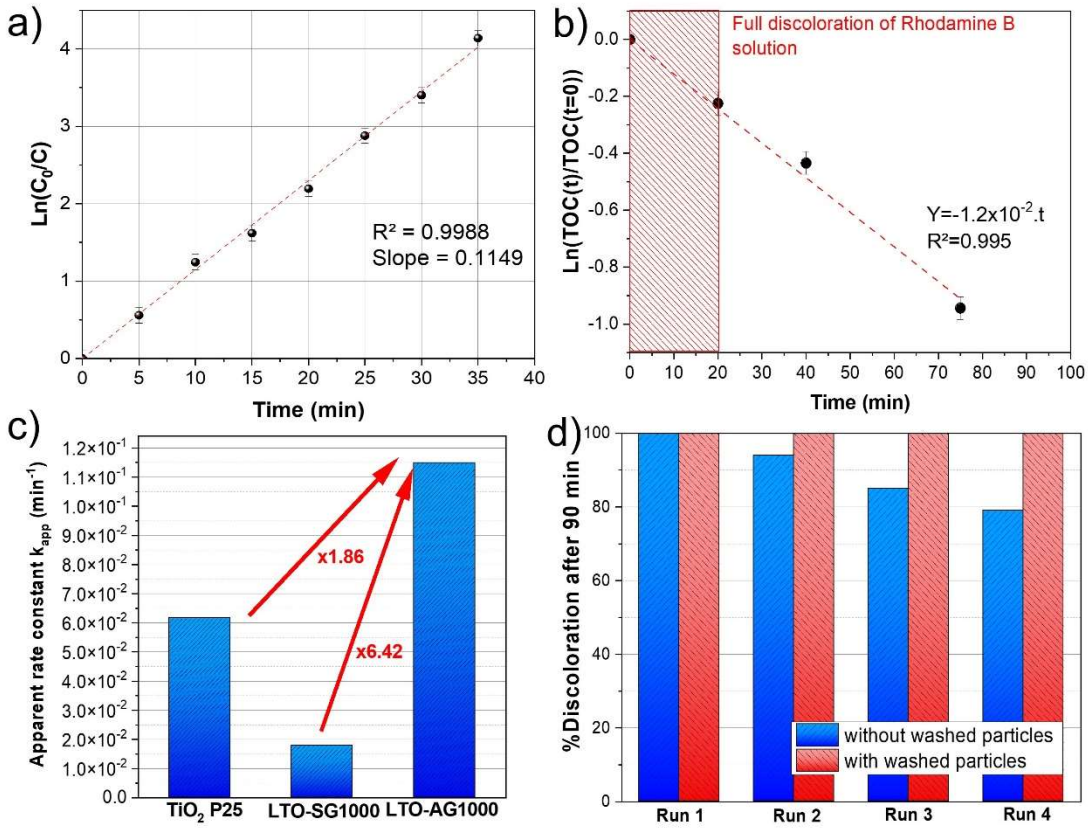

Figure 4.a) Example of Ln(C_0/C) vs Time plot to determine apparent rate constant for a sample of LTO-AG-1000 ; b) Total Organic Carbon analysis on the degradation of Rhodamine B with LTO-AG-1000 ; c) Photocatalytic efficiency of TiO_2 P25, Sol-Gel and Assisted by glycine synthesis and d) Recyclability test of Rhodamine B with LTO-AG-1000 with the influence of intermediates of photodegradation.

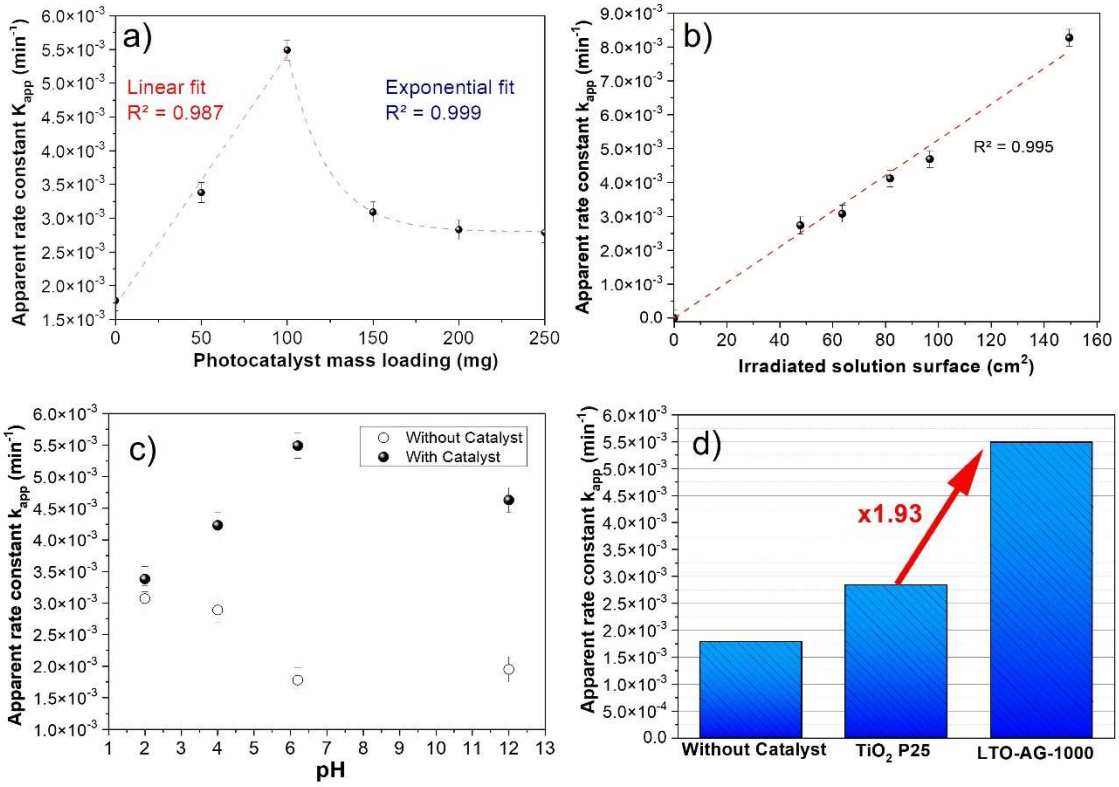

Figure 5.a) Evolution of apparent rate constant as function of catalyst loading with LTO-AG-1000 ; b) Evolution of apparent rate constant as function of irradiated surface with LTO-AG-1000 ; c) Evolution of apparent rate constant as function of pH with LTO-AG-1000 and d) Comparison of apparent rate constant without and with catalyst TiO_2 P25 and LTO-AG-1000.

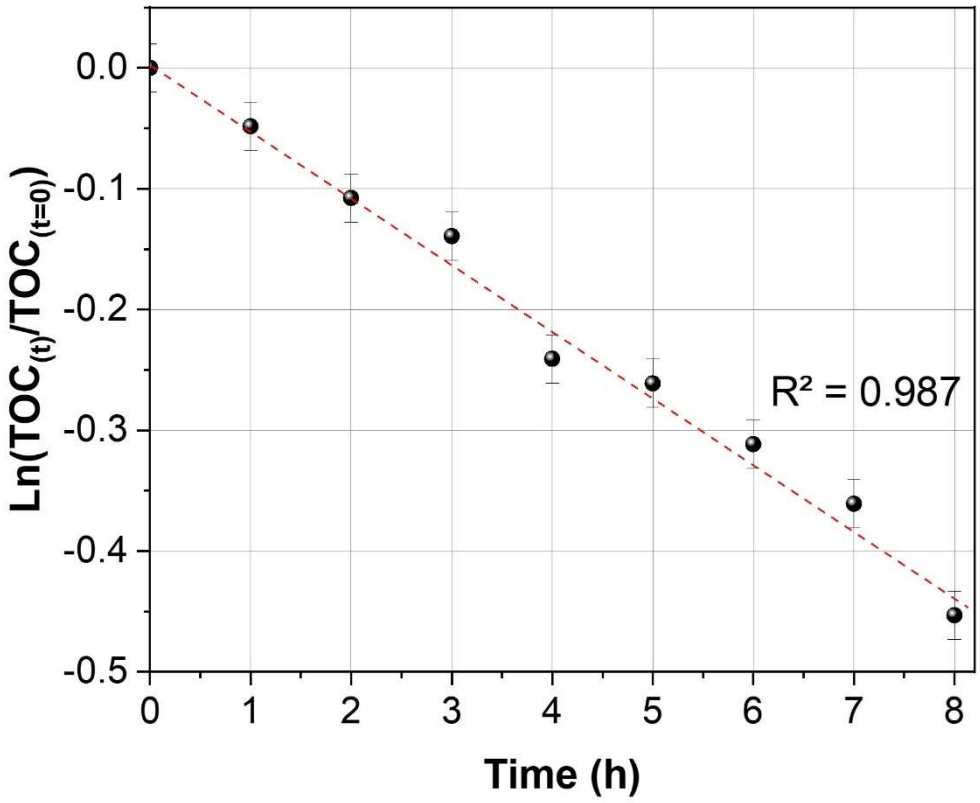

Figure 6. Total organic carbon analysis on the degradation of phenol with LTO-AG-1000.

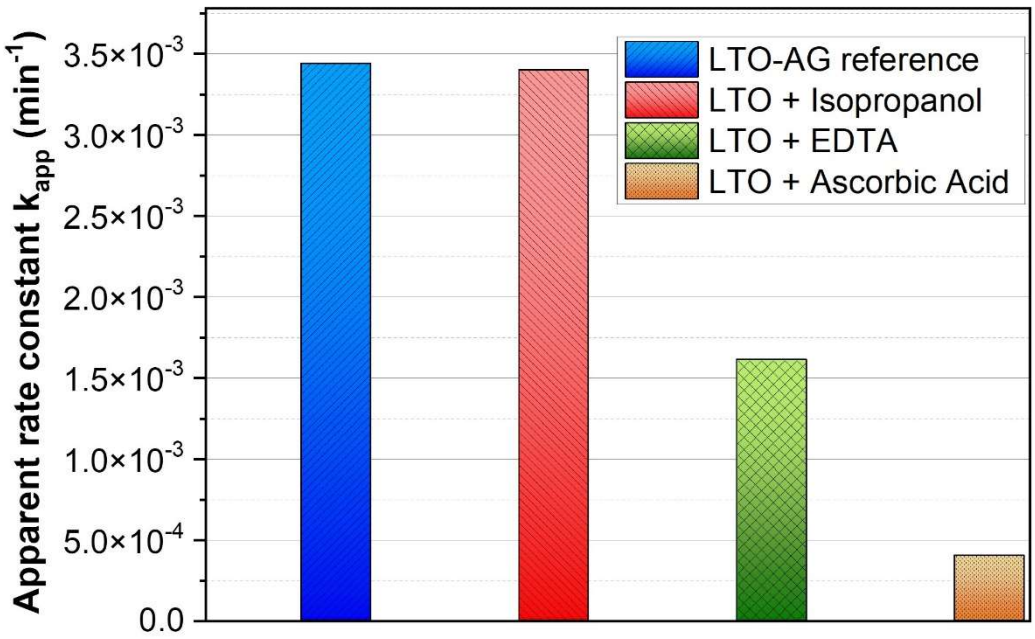

Figure 7. Influence of scavenger on the photocatalytic process with LTO-AG-1000.

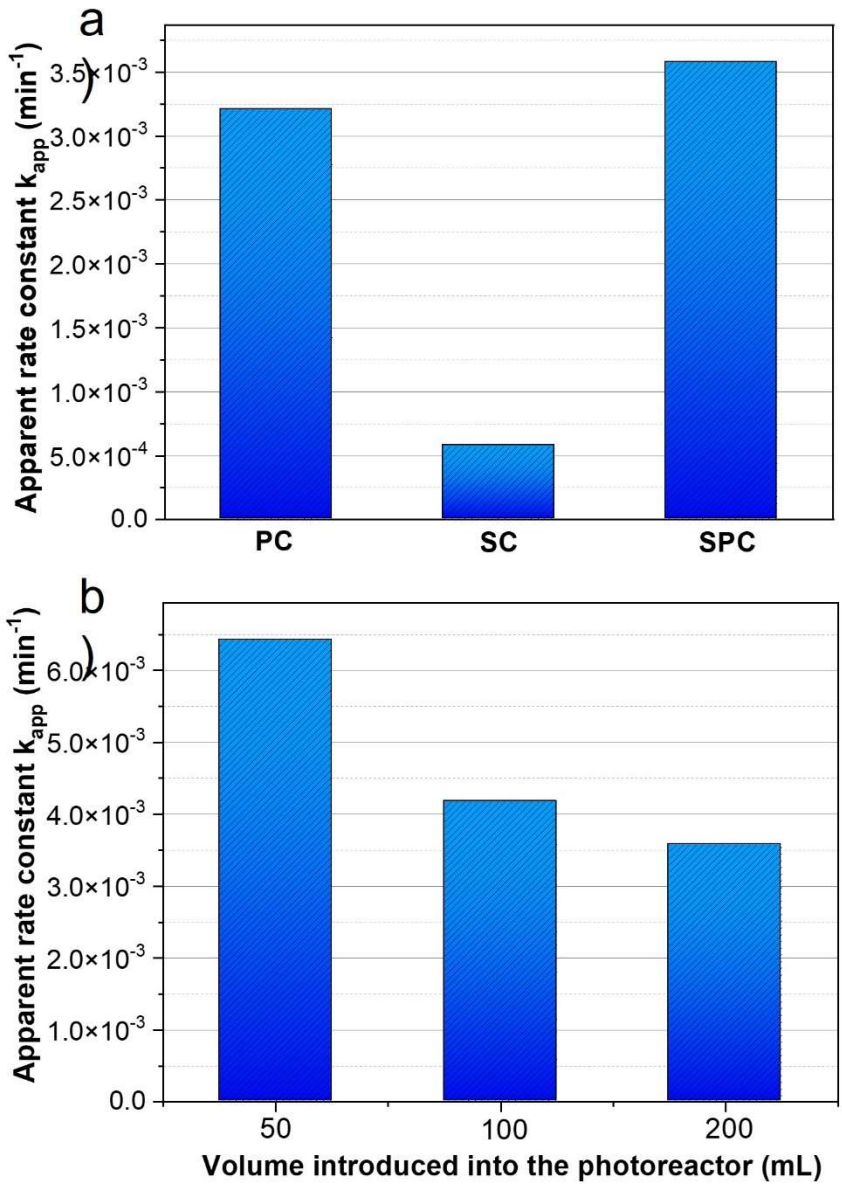

Figure 8.a) Histograms obtained for three effects, PhotoCatalysis (PC), SonoCatalysis (SC) and SonoPhotoCatalysis (SPC) for LTO-AG-1000 ; b) Influence of the volume to be sonicated on the photocatalytiv efficiency for LTO-AG-1000.